Mohammed J. Abdulameer
Mohammed A. Akraa

Department of Physics, College of Education for Pure Sciences, University of Babylon, Al-Hilla, Babil, IRAQ

Synthesis and Analysis of ZnO/CdS Nanocomposites: Structural and Optical Properties

This research investigates the structural and optical properties of ZnO/CdS nanocomposite synthesized through co-precipitation. Various analytical techniques, including x-ray diffraction (XRD), field-emission scanning electron microscopy (FE-SEM), Fourier-transform infrared spectroscopy (FTIR), and energy-dispersive x-ray spectroscopy (EDX), confirmed the formation of a pure, homogeneous nanocomposite. XRD analysis indicated that the compound is semi-crystalline with a crystalline size of approximately 9 nm. FESEM imaging showed that the ZnO/CdS nanocomposite has a spherical morphology. Ultraviolet-visible spectroscopy revealed a specific band gap value of 3.78 eV, corresponding to a wavelength of 328 nm. EDX analysis indicated the weight percentages of zinc, oxygen, cadmium, and sulfur to be 1.8%, 11.9%, 65.9%, and 20.5%, respectively. FTIR analysis identified functional groups confirming the presence of the desired compound.

Keywords: Nanoparticles; Optical properties; Chemical synthesis; ZnO/CdS
Received: 24 July 2024; Revised: 24 August; Accepted: 31 August 2024

1. Introduction

The increasing claim for capable and intelligent nanocomposite materials is driven by their distinct properties, along with their prospective applications in areas such as optoelectronics, catalysis, and biology [1-5]. Recent progress in materials design has greatly expedited the development of semiconductors by utilizing the combined benefits of their component materials. Zinc oxide (ZnO), in particular, extensive research has been conducted on its combination with other materials, including Co_3O_4, ZnS, CdS, TiO_2, CuO, SnO_2, and ZnSe, revealing significant applications [6-13].

CdS, with its narrow band gap of 2.42 eV and a conduction band edge slightly above that of ZnO, is an ideal candidate for combination with ZnO. The ZnO/CdS composite system has attracted considerable interest due to its unique properties and potential applications in photocatalysis and antibacterial activity [14-17]. Nanocomposites visible light photocatalysts like ZnO/CdS are effective because charge transfer between semiconductors enhances charge separation, thereby minimizing exciton recombination [18,19]. Moreover, the morphology and surface characteristics significantly influence the photocatalytic efficacy, as the catalytic reactions predominantly occur on semiconductor surfaces[20].

Concurrently, antibiotic resistance poses a critical challenge to public health, necessitating alternative antimicrobial strategies. Nanoparticles, owing to their high bioactivity and large specific surface area, are emerging as promising biomedical materials with enhanced antibacterial properties against multidrug-resistant pathogens, thereby meeting the escalating hygiene demands in various sectors. With their distinct morphologies, metal-oxide nanocomposites combine their constituent elements' beneficial properties to exert synergistic effects [21].

The development of materials with photocatalytic and antimicrobial properties is especially important. ZnO/CdS nanocomposites have shown significant potential as efficient photocatalyst's for decomposing organic pollutants under visible light and as powerful antimicrobial agents. The antibacterial efficacy of ZnO/CdS systems has been evidenced by their ability to completely deactivate bacteria under visible light irradiation. Moreover, there is increasing interest in antibacterial materials that maintain their activity and sustainability even in the absence of light [22,23].

In this study, we are focused on finding a photocatalyst that works within the ultraviolet range and is manufactured by coprecipitation method.

The coprecipitation technique was chosen for its affordability, high productivity, accurate compositional control, uniform particle size distribution, increased reactivity, ease of scaling, and adaptability.

We employed XRD, FE-SEM, FTIR, and EDX techniques to analyze the structural and optical properties of the synthesized ZnO/CdS nanocomposite, and evaluate its effectiveness in nano-antibacterial applications.

2. Experimental Part

Cadmium nitrate tetrahydrate [$Cd(NO_3)_2.4H_2O$] with molecular weight (M.W.) of 308.47 g/mol and sodium sulfide [Na_2S] with M.W. of 78.04+aq were supplied by Thomas Baker Chemicals (India). Zinc nitrate hexahydrate [$Zn(NO_3)_2.6H_2O$] with M.W. of 297.48 g/mol, sodium hydroxide [NaOH] with M.W. of 40.00 g/mol and thiourea [$NH_2.CS.NH_2$] with M.W. of 76.12 g/mol were supplied by LOBA Chemie (India).

The ZnO/CdS nanocomposites were synthesized using the coprecipitation method. Initially, 0.1 M (1.8 g) of $Zn(NO_3)_2.6H_2O$ and 0.2M (0.8 g) of NaOH were each dissolved in 100 mL of deionized water at room

temperature. The NaOH solution was then added to the $Zn(NO_3)_2.6H_2O$ solution, leading to the formation of a white ZnOH precipitate.

In the second step, 0.8 M (6 g) of thiourea was added to the previous solution, which was then heated to 80°C for 2 hours to form ZnS. Subsequently, 0.8 M (18.9 g) of $Cd(NO_3)_2.4H_2O$ and 0.8 M (6.24 g) of Na_2S were added to the ZnS solution, with each solution being dissolved in 100 mL of deionized water. After half an hour, the solution turned orange and was left to settle for 48 hours.

The resulting ZnO/CdS was washed with ethanol and deionized water three times each, using centrifugation for 20 minutes at 4000 rpm. The nanomaterial was dried at 60°C for 48 hours to obtain the solid powder of ZnO/CdS.

The Fourier-transform infrared (FTIR) spectra of the ZnO/CdS nanocomposite were obtained using a Perkin Elmer-Spectrum One spectrophotometer with the KBr pellet method. The crystalline nature of the sample was assessed via x-ray diffraction (XRD) with a PANalytical XPERT PRO MPD, Netherlands, over an angular range of 2θ=7-79.9° using Cu Kα radiation (λ=0.15418nm). The morphology was analyzed using an FEI Inspect F50 field-emission scanning electron microscope (FE-SEM), and elemental composition was determined by energy-dispersive x-ray spectroscopy (EDX) using Axia Chemi SEM from Thermo Scientific.

3. Results and Discussion

To characterize the structural and optical properties of the synthesized ZnO/CdS nanocomposites, a comprehensive analytical approach is employed. The XRD pattern is utilized to determine the crystalline phase and size of the nanocomposites, while the FE-SEM provides insights into their surface morphology and particle size distribution. The EDX is used to confirm the elemental composition and uniformity of the nanocomposites. The FTIR offers information about the functional groups and bonding environment within the material, and UV-visible spectroscopy helps in assessing the optical properties, such as bandgap energy and absorbance characteristics.

This multi-faceted characterization approach enables a thorough understanding of the ZnO/CdS nanocomposites, providing valuable insights into their potential applications and performance in various technological applications.

The results obtained from these analytical techniques are critical for evaluating the quality and effectiveness of the synthesized nanocomposites and for guiding future research and development in this field.

Initially, in this work, the XRD diagnosis exhibits the components of the ZnO/CDs composites in Fig. (1). The XRD analysis was conducted using Jade 6 software, developed by Materials Data, Inc.

The diffraction peaks at 31.8°, 34.4°, and 47.9° correspond to the Miller indices (100), (002), and (102), respectively, and are indexed to the hexagonal wurtzite phase of ZnO (ICDD file no. 36-1451). Additionally, the prominent diffraction peaks at 26.4°, 30.2°, 43.7°, and 51.7° are associated with the Miller indices (111), (200), (220), and (311), respectively, which correspond to the cubic CdS (ICDD file no. 89-0440) The parameters for the ZnO/CdS nanocomposites are detailed in table (1).

The significant broadening of the diffraction peaks suggests the formation of a nanophase. The crystallite size (D) was determined using the Debye-Scherrer equation [24]:

$$D = \frac{0.9\,\lambda}{\beta cos\theta} \quad (1)$$

where λ, β and θ are the wavelength of the radiation, the full-width half maximum (FWHM) of diffraction peak and the Bragg's angle, respectively. The average crystallite size of ZnO/CdS nanoparticles was 9 nm.

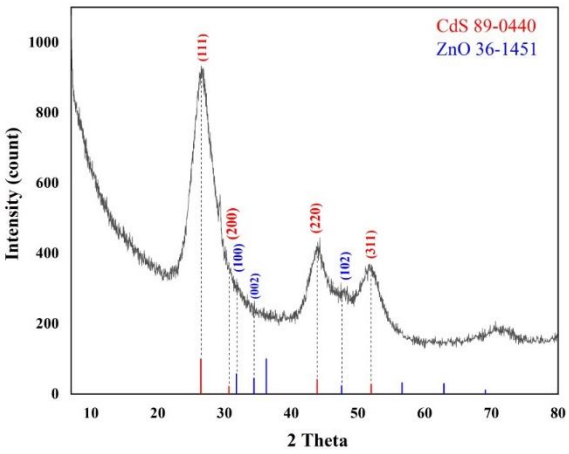

Fig. (1) XRD patterns of the ZnO/CdS nanocomposite

Table (1) The results obtained from XRD of ZnO/CdS NCs

2θ (deg)	Phase ID	hkl	ds_{pacing} (nm)	FWHM (deg)	Crystallinity size (nm)
26.4	CdS	(111)	0.3363	0.902	9.45
31.8	ZnO	(100)	0.2811	0.212	40.71
34.4	ZnO	(002)	0.2599	0.171	50.8
30.2	CdS	(200)	0.2948	0.176	48.8
47.9	ZnO	(102)	0.1894	0.319	28.4
43.7	CdS	(220)	0.2067	0.847	10.5
51.7	CdS	(311)	0.1765	0.730	12.6

The morphological characteristics of ZnO/CdS nanocomposite were analyzed via FE-SEM. The FE-SEM image in Fig. (2) reveals a spherical morphology for ZnO/CdS structures, with average particle sizes about 15 nm. These particle sizes are notably larger than the crystallite sizes previously determined by XRD (9 nm), indicating the aggregation of multiple crystallites. Particle size distribution for ZnO/CdS nanocomposite is presented in Fig. (2).

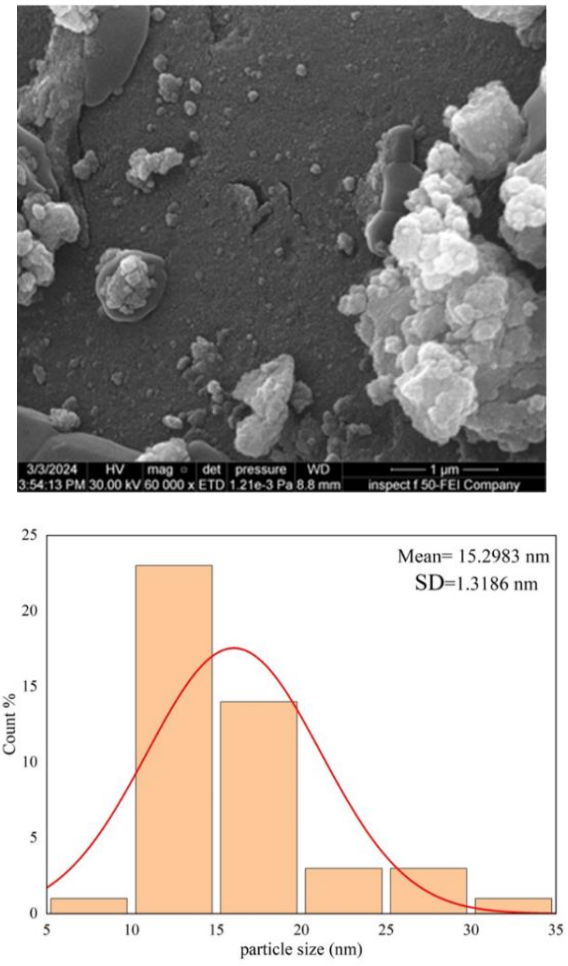

Fig (2) FE-SEM image and particle size distribution for ZnO/CdS nanocomposite fitted with a log normal distribution function

To corroborate the chemical analysis of ZnO/CdS nanocomposite, EDX was employed. It utilizes a Si–Li solid-state detector to detect characteristic x-rays emitted by atoms when excited by incident protons. Each element emits photons (x-rays) at specific energies, resulting in distinct peaks in the spectrum. The intensity of these peaks is proportional to the element's concentration, allowing for quantitative analysis (see Fig. 3). However, corrections must be applied considering sample composition and experimental parameters like incident beam energy and angle, limiting the analyses to semi-quantitative assessments in this study. The detection limit ranged from 0.1% to 1% for elements of average or low atomic weights, barring challenges from peak superposition.

The EDX spectrum in Fig. (3a) confirms the presence of zinc (Zn), oxygen (O), cadmium (Cd), and sulfur (S) elements, without any detectable impurities. Zn, O, Cd, and S weight percentages are 1.8%, 11.9%, 65.9%, and 20.5%, respectively, while the atomic percentages are 1.4%, 37.2%, 29.4%, and 32.0%, respectively.

The uniform distribution of these elements was further evidenced by elemental mapping conducted via FE-SEM, as depicted in figures (3b–f). This mapping demonstrates the even distribution of Zn, O, Cd, and S throughout the composite. These results provide substantial evidence of the uniformity and high purity of the synthesized ZnO/CdS composite.

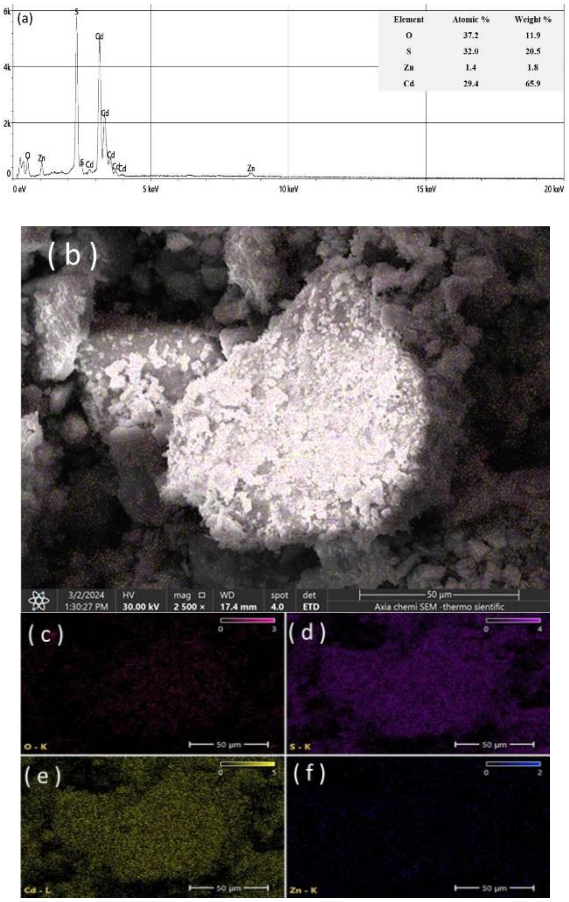

Fig. (3) (a) EDX spectrum and corresponding elemental mapping (b) CdS/ZnO (c) O, (d) S, (e) Cd and (f) Zn

The ZnO/CdS nanocomposite was analyzed using FTIR spectroscopy to identify the functional groups resulting from the precursor materials used in the co-precipitation synthesis. Within the range of 3757.35-3186.40 cm^{-1}, the peaks indicate O-H stretching vibrations, suggesting the presence of hydroxyl groups or water molecules. This can be attributed to the cadmium nitrate tetrahydrate and zinc nitrate hexahydrate used in the synthesis. Within the range of 2380.47-2177.82 cm^{-1}, the peaks correspond to C≡C or C≡N stretching vibrations, which may result from the thiourea or other reactive intermediates. In the range of 1872.82-1602.21 cm^{-1}, the peaks are attributed to C=N stretching vibrations, associated with carbonyl compounds such as aldehydes or ketones, possibly formed during the reactions involving thiourea. In the range of 1587.88-1382.98 cm^{-1}, the peaks indicate N=O bending vibrations, which are typical of primary or secondary amines, likely originating from thiourea. The range of 1110.00-669.85 cm^{-1} includes peaks corresponding to C-N and C-S stretching vibrations, indicating the

presence of functional groups from thiourea. Within the range of 519.92-473.95 cm^{-1}, the peaks are associated with Zn-O and Cd-S stretching vibrations, confirming the formation of ZnO and CdS in the nanocomposite [25].

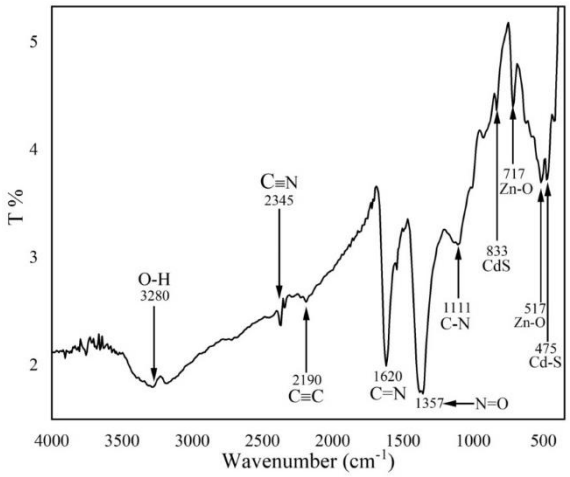

Fig. (4) FTIR spectra of ZnO/CdS nanocomposite

The optical properties of ZnO/CdS nanocomposites were investigated by the UV-visible spectrophotometry in the wavelength range of 200-1100 nm. The nanocomposite powder was dispersed with deionized water and placed in a cuvette with a 1 cm optical path length. Absorbance (A), absorption coefficient (α), and the optical bandgap (E_g) were determined and these values are depicted in Fig. (5).

The absorption coefficient of the sample can be determined by $\alpha = 2.303A/t$ [26], where A is the absorbance and t is the optical path length (1 cm). Consequently, the band gap energy (E_g) of ZnO/CdS nanocomposite was calculated using the Tauc relation, $\alpha h\nu \approx (h\nu - E_g)^{1/2}$ [27]. A plot of $(\alpha h\nu)^{1/2}$ versus $(h\nu)$ for the ZnO/CdS nanocomposite exhibited an indirect bandgap energy of the nanocomposite was found to be 3.78 eV, which corresponds a wavelength of 328 nm.

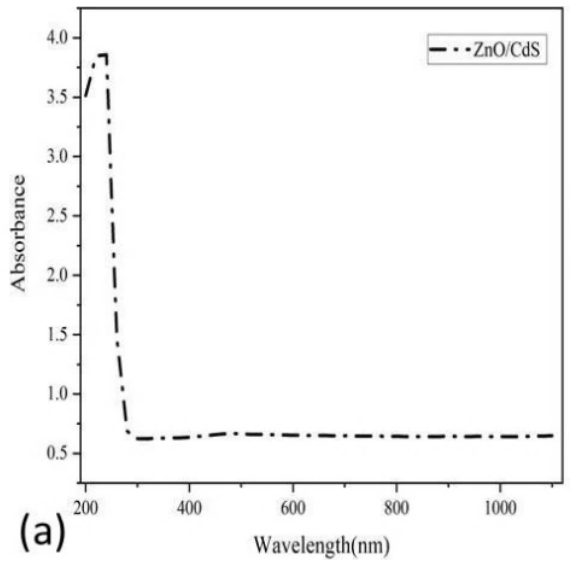

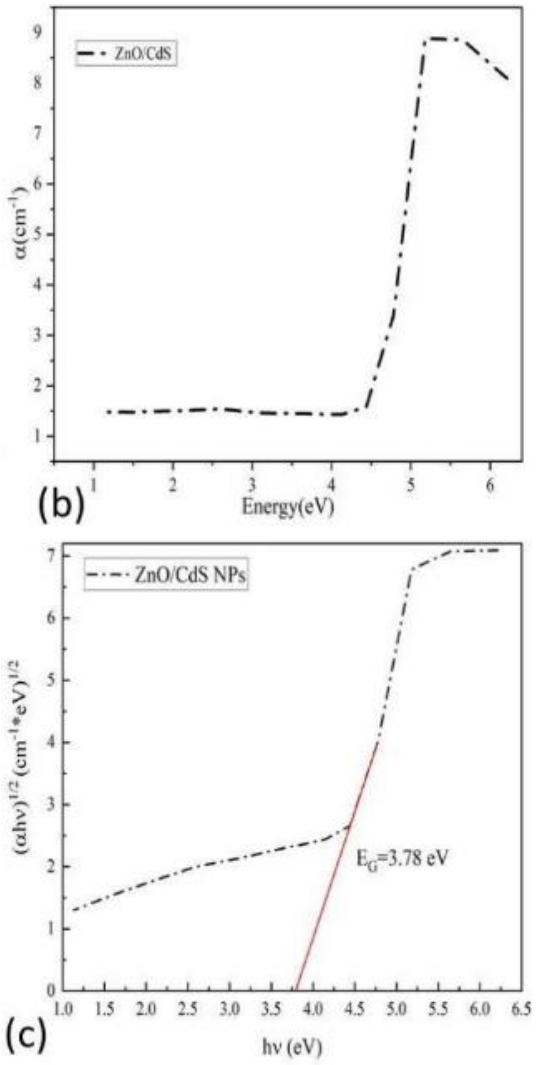

Fig. (5) (a) Absorbance, (b) absorption coefficient, and (c) indirect energy gap of ZnO/CdS nanocomposite

The quantum confinement effect resulting from nanoscale dimensions induces an increased band gap in ZnO/CdS nanocomposite. Interface interactions between these materials introduce new energy states that modify the band structure [28,29]. Additionally, surface chemical reactions occurring at interfaces or surfaces create additional energy levels that influence the overall band gap. Together, these factors collectively contribute to the observed higher energy band gap in ZnO/CdS nanostructures [30].

4. Conclusions

The co-precipitation method was utilized for the successful synthesis of ZnO/CdS nanocomposite powder. This material revealed a semi-crystalline structure and the average particle size was 9 nm. The formation of Zn-O and Cd-S bonds was confirmed. The structural purity of the prepared composite was demonstrated by the weight percentages of Zn, O, Cd, and S being 1.8%, 11.9%, 65.9%, and 20.5%, respectively, as well as the atomic percentages of 1.4%, 37.2%, 29.4%, and 32.0%, respectively. The band gap of the ZnO/CdS nanocomposite was

determined to be 3.78 eV, which is equivalent to an absorption edge of 328 nm. These results for ZnO/CdS nanocomposite make it a promising material in wide applications as light conversion, solar cells, and antibacterial activity.

References

[1] S. Cao et al., "Band alignment engineering for improved performance and stability of ZnFe2O4 modified CdS/ZnO nanostructured photoanode for PEC water splitting", *Nano Energy*, 24 (2016) 25-31.

[2] M. Shekofteh-Gohari and A. Habibi-Yangjeh, "Ultrasonic-assisted preparation of novel ternary ZnO/AgI/Fe_3O_4 nanocomposites as magnetically separable visible-light-driven photocatalysts with excellent activity", *J. Colloid Interface Sci.*, 461 (2016) 144-153.

[3] R. Michal et al., "Photocatalytic properties and selective antimicrobial activity of TiO 2 (Eu)/CuO nanocomposite", *Appl. Surf. Sci.*, 371 (2016) 538-546.

[4] Y. Sun and Y. Xia, "Shape-controlled synthesis of gold and silver nanoparticles", *Science*, 298(5601) (2002) 2176–2179.

[5] Y.W.C. Cao, R. Jin and C.A. Mirkin, "Nanoparticles with Raman spectroscopic fingerprints for DNA and RNA detection", *Science*, 297(5586) (2002) 1536–154.

[6] Y. Wang et al., "3-Dimensional ZnO/CdS nanocomposite with high mobility as an efficient electron transport layer for inverted polymer solar cells", *Phys. Chem. Chem. Phys.*, 18(17) (2016) 12175–12182.

[7] R. Sánchez-Tovar et al., "ZnO/ZnS heterostructures for hydrogen production by photoelectrochemical water splitting", *RSC Adv.*, 6(36) (2016) 30425–30435.

[8] L. Zhu, M. Hong and G.W. Ho, "Hierarchical Assembly of SnO_2/ZnO Nanostructures for Enhanced Photocatalytic Performance", *Sci. Rep.*, 5(1) (2015) 1-11.

[9] T.K. Jana, A. Pal and K. Chatterjee, "Magnetic and photocatalytic study of Co_3O_4-ZnO nanocomposite", *J. Alloys Comp.*, 653 (2015) 338–344.

[10] J. Geng et al., "Facile route to Zn-based II-VI semiconductor spheres, hollow spheres, and core/shell nanocrystals and their optical properties", *Langmuir*, 23(20) (2007) 10286–10293.

[11] M.A. Gondal, A.M. Ilyas and U. Baig, "Pulsed laser ablation in liquid synthesis of ZnO/TiO_2 nanocomposite catalyst with enhanced photovoltaic and photocatalytic performance", *Ceram. Int.*, 42(11) (2016) 13151–13160.

[12] A. Ghosh and A. Mondal, "Fabrication of stable, efficient and recyclable p-CuO/n-ZnO thin film heterojunction for visible light driven photocatalytic degradation of organic dyes", *Mater. Lett.*, 164 (2015) 221–224.

[13] L. Wang et al., "*in situ* formation of a ZnO/ZnSe nanonail array as a photoelectrode for enhanced photoelectrochemical water oxidation performance", *Nanoscale*, 8(17) (2016) 9366–9375.

[14] W. Kim, M. Baek, and K. Yong, "Fabrication of ZnO/CdS, ZnO/CdO core/shell nanorod arrays and investigation of their ethanol gas sensing properties", *Sens. Actuat. B: Chem.*, 223 (2016) 599–605.

[15] S.S. Warule et al., "Decoration of CdS nanoparticles on 3D self-assembled ZnO nanorods: A single-step process with enhanced field emission behaviour", *Cryst. Eng. Comm.*, 17(1) (2015) 140–148.

[16] P. Huo et al., "Incorporation of N–ZnO/CdS/Graphene oxide composite photocatalyst for enhanced photocatalytic activity under visible light", *J. Alloys Comp.*, 670 (2016) 198–209.

[17] M. Zirak et al., "Vertically aligned ZnO@CdS nanorod heterostructures for visible light photoinactivation of bacteria", *J. Alloys Comp.*, 590 (2014) 507–513.

[18] Y. Tak et al., "Type-II CdS nanoparticle-ZnO nanowire heterostructure arrays fabricated by a solution process: Enhanced photocatalytic activity", *Chem. Commun.*, 38 (2008) 4585–4587.

[19] T.K. Jana, A. Pal and K. Chatterjee, "Self assembled flower like CdS-ZnO nanocomposite and its photo catalytic activity", *J. Alloys Comp.*, 583 (2014) 510–515.

[20] S. Kant et al., "Removal of malachite green and methylene blue by $Fe_{0.01}Ni_{0.01}Zn_{0.98}O$/polyacrylamide nanocomposite using coupled adsorption and photocatalysis", *Appl. Catal. B: Environ.*, 147 (2014) 340–352.

[21] P.D. Cozzoli, T. Pellegrino and L. Manna, "Synthesis, properties and perspectives of hybrid nanocrystal structures", *Chem. Soc. Rev.*, 35(11) (2006) 1195–1208.

[22] Q. Li et al., "Antimicrobial nanomaterials for water disinfection and microbial control: Potential applications and implications", *Water Res.*, 42(18) (2008) 4591–4602.

[23] V. Lakshmi Prasanna and R. Vijayaraghavan, "Insight into the Mechanism of Antibacterial Activity of ZnO: Surface Defects Mediated Reactive Oxygen Species even in the Dark", *Langmuir*, 31(33) (2015) 9155–9162.

[24] H.K. Moudgil, **"TextBook of Physical Chemistry"**, PHI Learning (Delhi, 2010), Ch. 7, p. 261.

[25] P. Larkin, **"Infrared and Raman Spectroscopy: Principles and Spectral Interpretation"**, Elsevier (2011), Ch. 8, pp. 153-158.

[26] F. Urbach, **"The long-wavelength edge of photographic sensitivity and of the electronic Absorption of Solids"**, *Phys. Rev.*, 92(5) (1953).
[27] J. Tauc, "Optical Properties of Amorphous Semiconductors", in **"Amorphous and Liquid Semiconductors"**, Springer (Boston, 1974), pp. 159-220.
[28] G. Ali Mansoori, **"Principles of nanotechnology: Molecular based study of condensed matter in small systems"**, World Scientific Publishing Co. (2005).
[29] L. Jacak, P. Hawrylak and A. Wojs, **"Quantum Dots"**, Springer Science & Business Media (Berlin, 2013).
[30] V. Mote, Y. Purushotham and B. Dole, "Williamson-Hall analysis in estimation of lattice strain in nanometer-sized ZnO particles", *J. Theor. Appl. Phys.*, 6(1) (2012) 1–8.

